



# Cracking can make concrete stronger – The coupled effect of matrix cracking and SiO<sub>2</sub>-enhanced fiber/matrix interface healing on the tensile strength of FRCC

Bo Wu<sup>a</sup>, Yangqing Liu<sup>b</sup>, Peng Feng<sup>c</sup>, Jishen Qiu<sup>a,\*</sup>

<sup>a</sup> Department of Civil and Environmental Engineering, Hong Kong University of Science and Technology, 1 University Road, Clear Water Bay, Hong Kong, China

<sup>b</sup> Department of Civil Engineering, Shanghai University, 99 Shangda Road, Shanghai, China

<sup>c</sup> Department of Civil Engineering, Tsinghua University, Beijing, 100084, China

## ARTICLE INFO

### Keywords:

Autogenous healing  
Tensile strength recovery  
Fiber/cement interface  
Nano-SiO<sub>2</sub> coating  
FRCC

## ABSTRACT

It is a doctrine that cracking always degrades tensile properties of cementitious composites. This study first-timely demonstrates that in the presence of water, cracking can enhance the tensile properties of fiber-reinforced cementitious composites (FRCCs) via the autogenous healing of fiber/matrix interface. PVA micro-fibers with or without a layer of nano-SiO<sub>2</sub> coating were involved. Pre-debonding, water conditioning, and reloading were applied to single-fiber specimen made with both fibers. While both fibers engaged stronger the fiber-to-matrix frictional bond after water conditioning, the enhancement of SiO<sub>2</sub>-coated fiber was significantly larger as more healing product formed in-situ. Tensile pre-cracking, healing, and reloading were applied to FRCC specimens made with both fibers. While both fibers enabled FRCC tensile recovery via self-healing, only the FRCC with SiO<sub>2</sub>-coated fibers accomplished a higher tensile strength than their uncracked-but-identically-conditioned counterpart. Micromechanics-based modeling verifies that the enhanced FRCC tensile strength was due to healing-strengthened fiber/matrix interface.

## 1. Introduction

Concrete is a class of brittle cementitious composites. It is susceptible to cracking from drying shrinkage, thermal expansion/shrinkage, and most importantly mechanical loading. The cracks not only impair the mechanical performance but also deteriorate the environmental durability of concrete, because their presence accelerates the penetration of external agent, e.g., sulfates, carbonates, and chlorides [1–3]. Therefore, cracking has always been considered as a negative factor in concrete design. Different non-destructive technologies have been developed to detect the cracks so they can be repaired in time [4–6]; in recent years, a variety of functional agents, such as polymers [7,8] and mineral-precipitating bacteria [9,10] have been added in the mixture to enhance the self-healing ability in concrete.

In the presence of water, e.g., during the rain precipitation, a concrete crack can potentially heal itself without any functional agents, which is referred to as “autogenous healing” [11]. In this process, the formation of healing products mainly relies on the residual chemical reactivity of hydrated cement matrix. First, there would be unhydrated

clinkers in the matrix if the w/c ratio is lower than 0.36 (the minimum value to completely hydrate cement based on stoichiometry [12]); they can react with the water that penetrates through the crack, producing cement hydrates as the healing product [13]. Second, there are spare Ca<sup>2+</sup> ions in matrix pore solution; because of the ion concentration gradient, these ions would diffuse into the crack, where they can react with dissolved CO<sub>2</sub> to form CaCO<sub>3</sub> or just re-precipitate into Ca(OH)<sub>2</sub> as the healing products [14–16]. Essentially, autogenous healing represents a physio-chemical process where foreign matters (H<sub>2</sub>O or CO<sub>2</sub>) are added into concrete to produce new substances that have mechanical strength (the secondary cement hydrates, CaCO<sub>3</sub>, and/or Ca(OH)<sub>2</sub>). As the foreign matters penetrate significantly faster through a crack than they do in uncracked matrix [17–19], presence of cracks may accelerate this process of “addition”. Based on this reasoning, we intuitively ask a peculiar but perhaps important question: can cracking and the subsequent autogenous healing possibly make a concrete stronger than its counterpart that is never cracked but undergoes the same conditioning?

While the above reasoning seems logically sound and some studies have suggested the existence of this phenomenon [20–22], no study has

\* Corresponding author. Room 3577, Main Building, HKUST, 1 University Road, Clear Water Bay, Hong Kong Special Administrative Region of China.

E-mail address: [cejqiu@ust.hk](mailto:cejqiu@ust.hk) (J. Qiu).

<https://doi.org/10.1016/j.cemconcomp.2023.105011>

Received 8 August 2022; Received in revised form 27 November 2022; Accepted 26 February 2023

Available online 27 February 2023

0958-9465/© 2023 Elsevier Ltd. All rights reserved.

explicitly concluded that cracked-and-healed concrete can have an enhanced tensile strength, which can be attributed to two reasons. First, the residual reactivity of matrix cannot produce adequate healing products to close a common concrete crack, which is easily wider than 200 μm [15,23]; even if the crack width is controlled, for instance by micro fibers, to below 100 μm, only the shallow part of the crack can be filled [7,24,25]. Second, the studied matrix cracks are mostly Mode I fracture, i.e., the crack surface being normal to principal tensile stress; it means that even if the cracks are completely closed, the chemical bond between the healing product and the old matrix must be stronger than the matrix itself to induce higher tensile strength, which is unlikely.

Unlike conventional concrete, the fiber-reinforced cementitious composites (FRCCs) under tensile loading can generate two types of cracks: first, the tensile stress induces matrix cracks; then the bridging fibers start to take the tensile force, inducing interface crack between the embedded segment of the fiber and the matrix (often referred to as interface debonding). Previous studies have shown that if the matrix crack width is controlled by the fiber-bridging to 100 μm or finer, significant amount of autogenous healing products, e.g. CaCO<sub>3</sub> and/or Ca(OH)<sub>2</sub>, can form in situ [11,16] (Fig. 1a); a famous example of the matrix crack healing is seen in engineered cementitious composites (ECCs), a class of tensile strain-hardening FRCCs with ultrahigh ductility (1–5%) and extraordinary crack-controlling ability [26–28]. Recently, it was reported that CaCO<sub>3</sub> can also form in an interface crack between the fiber and the matrix (Fig. 1b) [29]. The interface healing is microstructurally distinct from the matrix healing in two ways. First, the interface crack (<<5 μm) is significantly finer than the matrix crack, which requires less amount of healing product [29]. Second, the interface crack is essentially a Mode II fracture, i.e., the crack is induced by the shear stress; it means that the mechanical strength can be provided by friction, and thus strong chemical bond between the healing product and crack surfaces is no longer critical. As a result, the interface healing,

which can enhance the fiber-bridging in ECC, should represent a better chance of the hypothetical cracking-and-healing-induced enhancement of concrete tensile strength.

Our previous work has demonstrated that the interface healing can induce stronger friction via single PVA fiber preloading-reloading test. However, higher tensile strength was not achieved in cracked-and-healed ECC specimens compared with the uncracked-and-identically-conditioned controls [29]. It was attributed to two reasons: first, the formation of CaCO<sub>3</sub> at the interface was hindered by the inadequate CO<sub>2</sub> supply to the internal part of ECC; second, many of the micro-fibers, which had a rather large aspect ratio (length  $L_f = 12$  mm, diameter  $d_f = 40$  μm,  $L_f/d_f = 300$ ), had been ruptured during pre-loading, so the healed interface could not contribute to tensile strength during reloading.

This work aims to achieve stronger tensile strength in cracked-and-healed FRCCs than uncracked-and-identically-conditioned ones, by two microstructural alterations that maximize the effect of interface healing. First, sol-gel method was conducted to coat a thin layer of nano-SiO<sub>2</sub> to the fiber surface, which can react with Ca<sup>2+</sup> to form C–S–H as interface healing products in the absence of CO<sub>2</sub> [30,31]; second, the micro-fiber aspect ratio ( $L_f = 18$  mm,  $d_f = 200$  μm,  $L_f/d_f = 90$ ) was reduced to minimize the fiber rupture. The experimental results enable us to reach the conclusion that it is possible, if water is consistently available, to engage a higher FRCC tensile strength by slightly pre-cracking it. Recently, a new FRCC fiber-bridging model has been developed based on the classic micromechanics-based theoretical framework [26] to calculate the post-healing tensile stress vs. crack width behavior [32]. This new model is able to determine the effect of interfacial enhancement and fiber pullout/rupture on the fiber-bridging behavior. Therefore, it was used to examine the experimental results – if enhanced FRCC tensile strength was seen, is it because of interface healing?

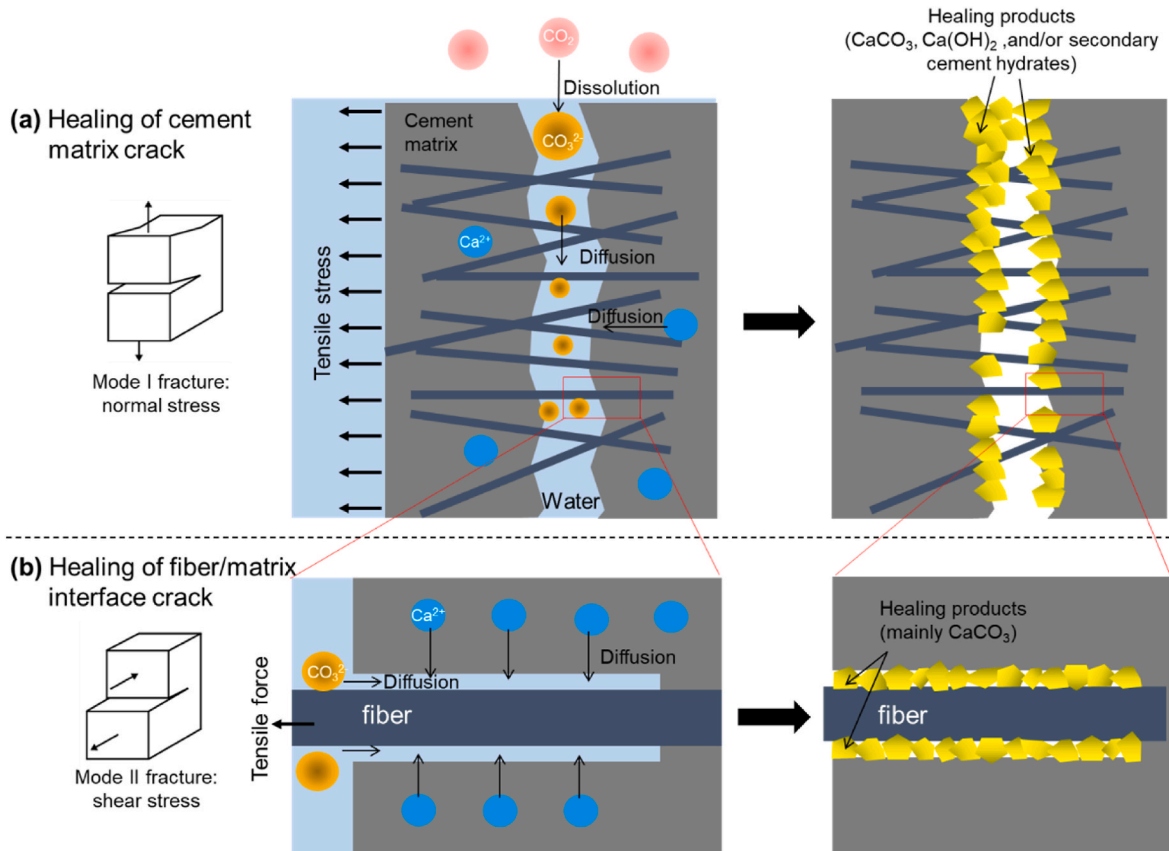


Fig. 1. Autogenous healing in FRCCs (esp. ECC) in the presence of water: (a) the healing of cement matrix crack; (b) the healing of fiber/matrix interface crack.

2. Experimental program

The experimental program of this study is summarized in Fig. 2. Micro-fibers were first coated with SiO<sub>2</sub> nanoparticles (Fig. 2a). The pristine or coated PVA fibers were used to make single-fiber pullout specimens (Fig. 2b) and notched dumbbell FRCCs specimens (Fig. 2c); the two specimen types were tested under uniaxial tension to determine the fiber/matrix interface bond and fiber-bridging strength,

respectively. In order to study the effect of pre-cracking and healing, the single-fiber and dumbbell specimens were pre-loaded and conditioned under different environments before reloading them to failure (Fig. 2d); another two testing protocols, i.e., directly loading the specimens with or without water conditioning to failure, were added as control groups. Besides the mechanical tests, multiple material characterization technologies were used to examine the microstructure and composition of fiber surface and fiber/matrix interface at different stages of the

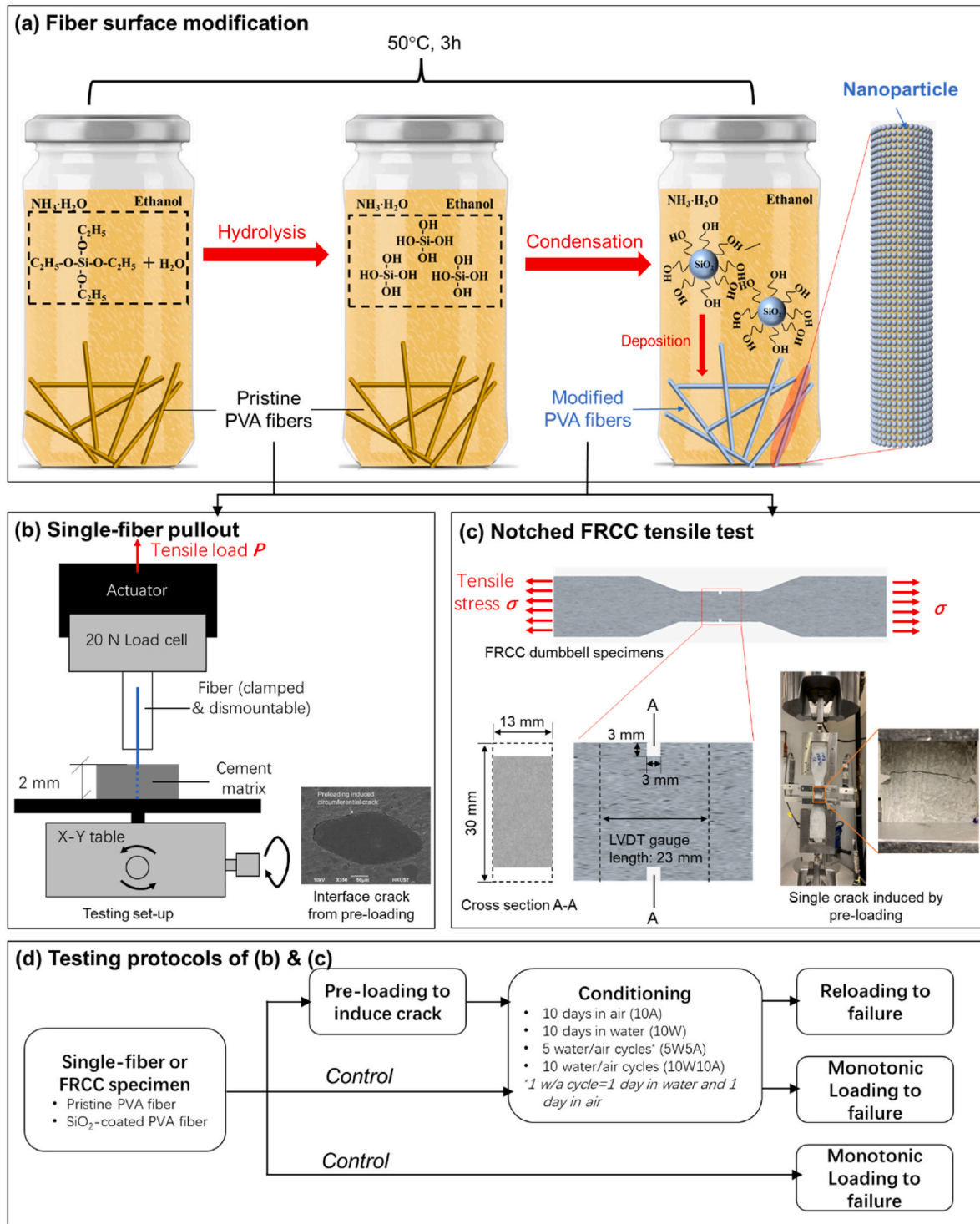


Fig. 2. Summary of the experimental program of this study: (a) method of modifying the surface of PVA micro-fibers with SiO<sub>2</sub> nanoparticles; (b) testing set-up of single-fiber pullout test, which is to examine the fiber/matrix interface bond; (c) testing set-up of the notched FRCCs tension, which is to examine the fiber-bridging strength; (d) testing protocols of the single-fiber pullout and FRCCs tensile tests.

experiment (Fig. 2d). The details of the experimental procedures are given as follows.

### 2.1. Fiber surface modification with nano-SiO<sub>2</sub>

In this study, polyvinyl alcohol (PVA) micro-fibers were selected to make single-fiber pullout specimens and FRCCs. The basic properties of the PVA fibers are given in Table 1. The fibers were received as in bundles, so they were first separated from each other by magnetic stirring (150/rpm) and ultra-sonication (750 W, 30% amplitude) in water for 15 min [33]. The soaked fibers were oven-dried at 70 °C for 8 h, which would not change the composition of the PVA. Then the dry fibers were treated in a sol-gel method (Fig. 2a) to grow SiO<sub>2</sub> nanoparticles on their surface. Specifically, 20 ml tetraethyl orthosilicate (TEOS) and 40 ml ammonia were dissolved into a binary solvent consisting of 450 ml ethanol (purity >99.5%) and 40 ml deionized water at 50 °C to synthesize SiO<sub>2</sub> nanoparticles. The chemical reaction involved two steps, i. e., the hydrolysis of TEOS to form H<sub>4</sub>SiO<sub>4</sub> and the condensation of H<sub>4</sub>SiO<sub>4</sub> under the catalysis by NH<sub>4</sub>OH to form SiO<sub>2</sub> nanoparticles [30, 34]. Then approximately 15 g pristine PVA fibers were added into the solution and kept under this temperature for 3 h to allow the nanoparticles being deposited onto the PVA surface. The processed fibers were collected by filtration, washed with deionized water for three times, oven-dried at 70 °C for 8 h before testing.

Both the pristine and processed PVA fibers were examined by scanning electron microscope (SEM, JEOL-6390), energy dispersive spectrometer (EDS, QUANTAX 4010), and X-ray photoelectron spectroscopy (XPS, PHI 5600). For examining the reactivity of coated SiO<sub>2</sub> in cement matrix, both fibers were immersed in saturated Ca(OH)<sub>2</sub> solution, which simulates the environment in the pore solution of cement paste [35], to grow hydration products. Specifically, the fibers were conditioned in saturated Ca(OH)<sub>2</sub> solution that is hermetically sealed in glass vial to prevent contact with CO<sub>2</sub>; the conditioning was under room temperature for three days. Then the fibers were removed from the vial, rinsed with deionized water for three times, and oven-dried at 70 °C for 8 h. The same SEM-EDS facility was used to characterize the products that formed on fiber surface.

### 2.2. Single-fiber pullout test

Single fiber pull-out tests (Fig. 2b) were conducted to determine the fiber/cement interfacial properties. To fabricate the single fiber specimen, a fresh cement paste (Type I OPC, 52.5 R, water/cement ratio of 0.35) was cast into a shallow mold holding multiple fibers that stick out by about 7 mm. These multi-fiber cement blocks were demolded after 24-h ambient curing, and further cured under 22 ± 3 °C and 95% relative humidity for another 27 days. After that, the blocks were cut into single fiber specimens of a small thickness (2 ± 0.2 mm). The mechanical loading to the single fiber specimens was conducted with an electrical universal material testing machine (Lyllod, model EZ50) equipped with a 20 N load cell and a displacement-controlled actuator. In this test setup, the cement block was glued to the X–Y table beneath, while the fiber tip was clamped to a metal plate at the top [36]. The loading rate for all these tests was set at 0.5 mm/min.

For both the pristine and processed single-fiber specimens, three loading protocols were applied. In the first protocol, the fiber was monotonically pulled out by a uniaxial tensile loading right away (group tag: 0W); in the second protocol, the fiber was conditioned in water for 10 days and then monotonically pulled out (10W). These two protocols

**Table 1**  
Properties of the PVA fibers used in this study.

Length (mm)	Diameter (μm)	Density (kg/m <sup>3</sup> )	Tensile strength (MPa)	Young's modulus (GPa)
18	200	1300	1000	27

serve as controls for the third one. In the third protocol, the fiber was first pre-loaded and stopped when a sudden and major load drop is observed, which denoted the full fiber/cement debonding [36]; then the specimen was dismantled from the setup and conditioned in four different environmental regimes (22 ± 3 °C) to engage autogenous healing, including (1) 10 days in ambient air (P10A, where P stands for pre-loading), (2) 10 days in water (P10W), (3) 5 wetting-air cycles, each consisting of one day in water followed by one day in air (P5W5A), (4) 10 wetting-air cycles (P10W10A); finally, the healed specimen was re-loaded to pull out the fiber. For each group (fiber type and loading/condition protocol), at least 5 single-fiber specimens were tested.

After the mechanical test, the fiber segment previously embedded in cement was examined under SEM-EDS. To determine the healed interface, the cross section and longitudinal interface zone of the healed specimen was consecutively polished by 400, 1200 and 2000 mesh sand paper and then immersed in isopropanol before subjecting to SEM-EDS characterization.

### 2.3. Tensile test of notched FRCC

FRCCs tensile tests (Fig. 2c) were conducted to determine the fiber-bridging strength of the composites. To prepare FRCCs specimens, 2 vol % pristine or processed fibers were added into the same fresh cement paste used for single-fiber specimen, followed by mixing in a Honart™ HL 400 mixer until the fiber was evenly distributed. After mixing, the fresh FRCC was cast into dumbbell molds. The specimens were cured in air for 24 h prior to demolding; after that they were moved into a moisture room with the temperature of 22 ± 3 °C and relative humidity of 95 ± 5% for other 27-day curing. Before mechanical test, two notches were made at the middle point of the specimen, which ensured that during pre-loading only one crack would appear within the gauged length. Two LVDTs were attached to the specimen by holders clamped onto it, the resultant gauge length was 23 mm. The mechanical loading to the notched FRCC specimens was carried out with a hydraulic universal material testing machine (MTS, model 810). Uniaxial tensile load was applied to the FRCC specimens at a rate of 0.3 mm/min to induce single crack. The crack opening was determined by the two LVDTs.

For the FRCCs made with both pristine and processed fibers, two loading protocols were applied. In the first one, the FRCCs specimen was conditioned for 10 wetting-air cycles (10W10A) and then monotonically loaded under uniaxial tension to failure; it serves as the control of the second protocol. In the second one, the FRCCs specimen was first pre-loaded until a single crack was seen in the neck (for all tested specimens the tensile strain of the gauged length was within the range of 1.3%–1.7%); then the specimen was dismantled and conditioned in two different environmental regimes (22 ± 3 °C) to engage autogenous healing, i.e., including (1) 5 wetting-air cycles, each consisting of one day in water followed by one day in air (P5W5A) and (2) 10 wetting-air cycles (P10W10A); finally, the healed specimen was re-loaded under uniaxial tension to failure. For each group (fiber type and loading/condition protocol), at least 3 FRCC specimens were tested.

After failure of the reloading PVA-SiO<sub>2</sub> specimen, the fracture surface was detected by optical image and SEM to determine the integrity of the fiber. A fragment of the specimen near the fracture surface was taken out by cutting, which was then polished by sand papers (400, 1200 and 2000 mesh) to expose the longitudinal section of the embedded fiber, and kept in isopropanol prior to the SEM characterization.

### 2.4. Modeling of the post-healing tensile behavior of FRCC

To further clarify the experimental results, a newly-developed fiber-bridging model [32] was used to simulate the post-healing tensile behavior of FRCC. Based on the classic micromechanics-based two-way fiber-bridging model [26], this new model takes into account the fiber debonding, slippage and rupture during preloading, and the variation of fiber/matrix interface bond after healing. If a fiber has both healed and

pristine interface to the matrix, a two-stage debonding process is considered. More details of this model can be found in Ref. [37]. The tensile stress ( $\sigma$ ) vs. crack opening displacement (COD ( $d$ )) curves of the four groups, i.e., pristine-10W10A (monotonic), pristine-P10W10A (reloading), SiO<sub>2</sub>-10W10A (monotonic), and SiO<sub>2</sub>-P10W10A (reloading), were calculated. The involved parameters and corresponding values are listed in Table 2.

In new model the pre-loading tensile stress vs. COD curve was calculated first, then the COD corresponding to the last stress recorded during the pre-loading was taken as the  $d_{pre}$ . This is to minimize the influence of elastic deformation of matrix and the possible slippage between LVDT and FRCCs on crack width and the number of rupture fiber during pre-loading. The slip-hardening coefficient  $\beta$  was normally calculated from the slope of  $P$ - $u$  curve near the point ( $P_b, u_0$ ). However, this method seems to be subjective due to the unclear definition of “being near”. Therefore, the  $\beta$  or  $\beta_{new}$  was determined by the area under calculated  $P$ - $u$  curve when it is equivalent to the energy absorption ( $G_w$ ) calculated from experiment results at the same displacement (e.g.,  $u = 1$  mm).

### 3. Results and discussions

#### 3.1. Nano-SiO<sub>2</sub> coating and its effect on fiber surface reactivity and fiber/matrix bond

Fig. 3a and b compare the morphology, surface reactivity and interface bond between the pristine PVA fiber and the processed PVA fiber with SiO<sub>2</sub> coating. In the SEM images (Fig. 3a), the pristine PVA fiber shows a relatively smooth surface, while shallow longitudinal grooves from the uneven PVA shrinkage during fiber manufacture can still be observed [31,38]; only C and O are detected in EDS. The processed PVA fiber shows a grainy surface distinct from the pristine, most grains are between 100 nm and 500 nm; additional Si can be detected, which indicates SiO<sub>2</sub> nanoparticles have been successfully coated onto PVA fiber surface. Significant fraction of C is still present because the

SiO<sub>2</sub> coating is only a few hundred nanometers thick and the incident electron beam could reach several microns deep.

After being submerged in the oversaturated Ca(OH)<sub>2</sub> for three days, minor crystal-like particles have randomly precipitated over the pristine fiber surface, while the grooves are still present at most parts; traceable Ca (1.4 wt%) appears, which indicates the new precipitates are likely Ca(OH)<sub>2</sub> (less likely to be CaCO<sub>3</sub> as CO<sub>2</sub> was scarce in the sealed vial). In contrast, the Ca(OH)<sub>2</sub>-conditioned processed fiber surface has mostly been covered by a continuous layer of gel-like substance while only a small portion remains grainy, which indicates that the nano-SiO<sub>2</sub> has stronger reactivity than PVA in cement matrix; on this fiber, both Si (5.7%) and Ca (2.5%) are detected. The XPS results (Fig. 3b) shows the prominent Si2p peak (103.6 eV) of the PVA-SiO<sub>2</sub> sample, further proving a successful coating of SiO<sub>2</sub> nanoparticles onto PVA fiber. A small shift to lower binding energy (103.3 eV) can be observed after Ca(OH)<sub>2</sub> conditioning, which may be attributed to the calcium acts as a charge-balancing cation within C-S-H structure, leading to the higher residual negative charges on the silicate tetrahedra and lower binding energy of silica atoms [39,40]. It suggests that the SiO<sub>2</sub> coating and the Ca<sup>2+</sup> ions are chemically combined, and the resultant gel-like substance is likely C-S-H [30].

Fig. 3c compares the load vs. displacement ( $P$ - $u$ ) curves obtained from the single-fiber pullout test of pristine (group tag: PVA\_0W) and processed fiber (PVA-SiO<sub>2</sub>\_0W). Both specimens demonstrate the two signature stages [41], i.e., the fiber debonding stage as  $P$  ramping linearly and the fiber pullout stage where  $P$  gradually decreasing to zero as  $u$  reaches the fiber embedment length (~2 mm). The sudden load drop from  $P_a$  to  $P_b$  represents that fiber debonding from matrix, which starts from the surface to the deep part, has completed. The processed fiber has shown noticeably higher characteristic loads  $P_a$  and  $P_b$  than the pristine fiber.

Based on the measured characteristic loads  $P_a, P_b$ , and the work to induce an  $x$ -mm ( $x = 0.5, 1.0, \text{ and } 1.5$ ) fiber displacement  $W_x$  (e.g.,  $W_{1.0}$  is shown as the hatched area in Fig. 3c), the chemical bond  $G_d$ , frictional bond  $\tau_0$ , and the specific energy absorption  $G_{w-x}$  (hereafter

**Table 2**  
Input parameters of the fiber-bridging modeling.

Parameters		Pristine-10W10A	Pristine-P10W10A		SiO <sub>2</sub> -10W10A	SiO <sub>2</sub> -P10W10A	
		Monotonic	Pre-loading	Re-loading	Monotonic	Pre-loading	Re-loading
Basic property	Fiber Young's modulus $E_f$ (GPa) <sup>a</sup>	27					
	Equivalent fiber diameter $d_f$ ( $\mu\text{m}$ ) <sup>a</sup>	200					
	Fiber length $L_f$ (mm) <sup>a</sup>	18					
	Fiber in-situ tensile strength $\sigma_f$ (MPa) <sup>b</sup>	730					
	Fiber strength reduction coefficient $f^c$	0.3					
	Fiber snubbing coefficient $f^d$	0.8					
	Fiber vol. Fraction in FRCC $V_f$ (%) <sup>e</sup>	2					
	Matrix Young's modulus $E_m$ (GPa) <sup>e</sup>	8					
	Crack width caused by pre-loading $d_{pre}$ ( $\mu\text{m}$ ) <sup>f</sup>	–	–	70	–	–	90
Fiber-to-matrix interface property	Chemical bond (intact interface) $G_d$ ( $\text{J}/\text{m}^2$ ) <sup>g</sup>	5.97	4.28	5.97	14.79	9.55	14.79
	Frictional bond (intact interface) $\tau_0$ (MPa) <sup>g</sup>	0.99	0.88	0.99	1.26	1.10	1.26
	Slip-hardening coefficient (intact interface) $\beta^h$	0.14	0.15	0.14	0.32	0.19	0.32
	Chemical bond (debonded-healed interface) $G_{d,new}$ ( $\text{J}/\text{m}^2$ ) <sup>g</sup>	–	–	0	–	–	0
	Frictional bond (debonded-healed interface) $\tau_{0,new}$ (MPa) <sup>g</sup>	–	–	2.61	–	–	4.35
	Slip-hardening coefficient (debonded-healed) $\beta_{new}$ <sup>h</sup>	–	–	0	–	–	0.49

<sup>a</sup> Fiber properties provided by the manufacturer.

<sup>b</sup> Ref. [48] reports that the PVA fiber in-situ tensile strength is approximately 73% of the nominal fiber strength, which is 1000 MPa for the current PVA fiber.

<sup>c</sup> Ref. [47].

<sup>d</sup> Ref. [46].

<sup>e</sup> Based on the FRCC testing scheme in Section 2.3.

<sup>f</sup> Inversely calculated based on the last tensile stress recorded during the FRCC pre-loading.

<sup>g</sup> The  $G_d$  and  $\tau_0$  values from Table 3.

<sup>h</sup> Calculated from the  $G_{w-1.0}$  in Table 3.

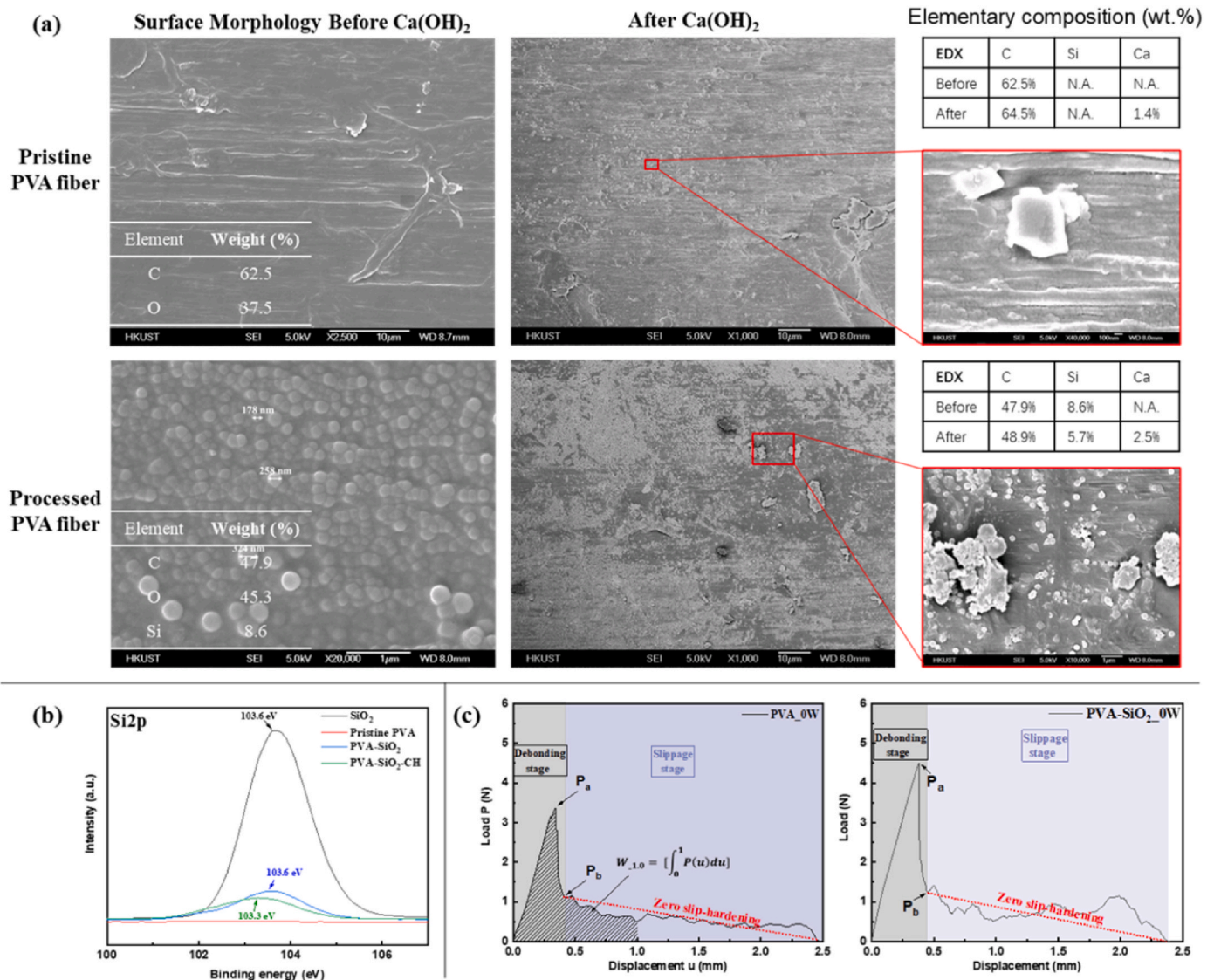


**Fig. 3.** Experimental results regarding the nano-SiO<sub>2</sub> coating on PVA fiber and its effect: (a) the surface morphology and elementary composition of pristine and processed PVA fiber, before and after the conditioning in oversaturated Ca(OH)<sub>2</sub>; (b) the Si2p spectra of processed PVA fiber; (c) the single-fiber pullout P-u curve of the pristine and processed fiber.

referred to as energy absorption) of the fiber/matrix interface can be determined with following equations [37,42]:

$$G_d = \frac{2(P_a - P_b)^2}{\pi^2 E_f d_f^3} \quad (\text{J} / \text{m}^2) \quad (1)$$

$$\tau_0 = \frac{P_b}{\pi d_f L_e} \quad (\text{MPa}) \quad (2)$$

$$G_{w-x} = \frac{W_x}{\pi d_f L_e} \quad (\text{J} / \text{m}^2) \quad (3)$$

where the  $E_f$ ,  $d_f$ , and  $L_e$  are Young's modulus, fiber diameter, and fiber embedment length, respectively. Here, the interface energy absorption instead was used as an indirect index to characterize the slip-hardening; directly calculating the slip-hardening coefficient, which must rely on measuring the slope of the P-u right after full fiber debonding, is not used here because the slope measurement is subject to subjectivity and can vary significantly.

The fiber/matrix interface properties obtained in current study, i.e.,  $G_d$ ,  $\tau_0$ , and  $G_{w-x}$ , are summarized in Table 3. As expected, the surface

coating significantly enhanced the fiber/matrix interface bond. The processed PVA fiber has doubled the chemical bond of the pristine fiber (9.55 vs. 4.28 J/m<sup>2</sup>), which is attributed to the refined interfacial micro porosity by the nano-SiO<sub>2</sub> coating [30,43]. Because of the stronger chemical bond, the debonded interface induced stronger friction and slip-hardening effect, and thereby larger energy absorption [30,44,45].

### 3.2. Healing-induced fiber/matrix interface recovery (w/or w/o nano-SiO<sub>2</sub> coating)

Fig. 4 shows the representative P-u curves of reloading the single-fiber specimen of different groups, which underwent the same pre-loading scheme (i.e., stop and release loading when P<sub>a</sub> dropped to P<sub>b</sub>) but had different fiber types and healing conditions. The interface properties of all the conditioned groups are summarized in Table 3.

Regarding the pristine fibers, air-only conditioning (Fig. 4a) induced no enhancement of the interface property, as shown by the almost unchanged P<sub>b</sub>' (compared with P<sub>b</sub>) and the P-u (compared with Fig. 3c). On the other hand, water-only conditioning (Fig. 4b) induced noticeable enhancement, as shown by the markedly higher P<sub>b</sub>' above P<sub>b</sub> and the P-u curve above the zero-slip-hardening line. Alternative air/water

**Table 3**

Fiber/matrix interfacial bond properties obtained from monotonic and preloading-reloading tests.

Fiber type	Group	$G_d^a$ (J/m <sup>2</sup> )	$\tau_0$ (MPa)	$G_{w-0.5}$ (J/m <sup>2</sup> )	$G_{w-1.0}$ (J/m <sup>2</sup> )	$G_{w-1.5}$ (J/m <sup>2</sup> )
Pristine PVA	0W	4.28	0.88 ± 0.12	604 ± 86	896 ± 123	1109 ± 154
	(monotonic)	± 0.78				
	10W	5.97	0.99 ± 0.38	701 ± 106	990 ± 192	1206 ± 211
	(monotonic)	± 3.09				
	P10A	0	0.87 ± 0.13	327 ± 70	567 ± 125	721 ± 129
	(reloading)					
	P10W	0	1.31 ± 0.12	426 ± 33	796 ± 23	1013 ± 48
	(reloading)					
	P5W5A	0	2.42 ± 0.15	400 ± 29	876 ± 187	1254 ± 284
	(reloading)					
Processed PVA	0W	9.55	1.10 ± 0.12	810 ± 134	1190 ± 217	1615 ± 260
	(monotonic)	± 2.20				
	10W	14.79	1.26 ± 0.36	1119 ± 118	1657 ± 22	2006 ± 4
	(monotonic)	± 1.31				
	P10A	0	0.91 ± 0.03	348 ± 36	681 ± 45	979 ± 48
	(reloading)					
	P10W	0	2.18 ± 0.16	870 ± 79	1775 ± 424	2724 ± 557
	(reloading)					
	P5W5A	2.18	1.16 ± 0.19	673 ± 16	1307 ± 195	1707 ± 270
	(reloading)	± 0.87				
P10W10A	0	4.35 ± 1.76	1564 ± 451	4698 ±	/	1630
(reloading)						

<sup>a</sup>  $G_d = 0$  means no sudden load drop ( $P_a$  to  $P_b$ ) was observed.

conditioning also enhanced the interface properties; the enhancement induced by 5 wetting/air cycles (Fig. 4c) is comparable to that by the water-only conditioning, while further enhancement was realized by 10 wetting/air cycles (Fig. 4d). However, no load drop from  $P_a$  to  $P_b$  was witnessed, indicating the chemical bond was not re-established at the debonded interface.

Regarding the processed fiber, air-only conditioning induced no interface enhancement (Fig. 4e), while the other three groups (Fig. 4f–4h) demonstrated an apparent recovery. It implies that the fiber/matrix interface healing is not negatively affected by nano-SiO<sub>2</sub> coating. Nevertheless, it should be noted that the coating could remarkably change the degree or manner of interfacial healing. For instance, the

sudden drop from  $P_a$  to  $P_b$  appeared after 5 wetting/air cycles (Fig. 4g), indicating that the re-establishment of chemical bond could be possible; after 10 wetting/air cycles (Fig. 4h), the  $P_b$  and the  $P-u$  curve during fiber slippage were enhanced so significantly that it changed the failure mode from fiber pullout to fiber rupture.

In Fig. 5, the interface properties ( $G_d$ ,  $\tau_0$ , and  $G_{w-1.0}$ ) obtained with the reloading (group tag: PxWyA) curves were normalized by the same property obtained from the monotonically loaded control groups (0W and 10W), to quantify the degree of interface healing. First, the comparison between 0W and 10W quantify the effect of continuous hydration on the interface properties. Expectedly, the continuous hydration significantly increased the chemical bond  $G_d$ , but only slightly, if any, increased the frictional bond  $\tau_0$  and energy absorption  $G_{w-1.0}$ . If a FRCC specimen is conditioned in water for 10 days, the internal fiber/matrix interface properties may decrease with its distance to the surface because of the decreasing hydration degree; however, all the properties should fall between the upper limit set by 10W and the lower limit set by 0W. In other words, in Fig. 5 the value normalized by 10W represents the minimum possible healing degree, while that by 0W represents the maximum possible healing degree.

The fiber/matrix interface healing degree is evaluated by the recovery of  $G_d$  and enhancement of  $\tau_0$  and  $G_{w-1.0}$ . The normalized  $G_d$  of almost all the groups are zero (Fig. 5a and d). This indicates that it is difficult to establish chemical bonds between the healing products and hardened matrix, even if the crack width was sufficiently fine (<1 μm) and the fiber surface reactivity is high (the nano-SiO<sub>2</sub> coating). These results agree with the conclusions of [29], which re-highlights the importance of enhancing frictional bonds during the conditioning. In terms of  $G_d$  recovery, the only exception is the group of SiO<sub>2</sub>-P5W5A, which had a minor  $G_d$  recovery of 15–23%. Fig. 6 compares the microstructure of the debonded-and-conditioned (5W5A) interface at the pristine fiber and that at the SiO<sub>2</sub>-coated fiber. It is seen that interface crack width of the two samples were both approximately 1 μm; however, in absence of nano-SiO<sub>2</sub> coating, the filling of the crack was incomplete.

Fig. 5b–c and 5e–f clearly show that the water-involved conditioning could enhance frictional bond and energy absorption of the debonded interface, which can even be higher than their undebonded controls. However, the enhancements of the pristine fibers are not as pronounced as the processed fibers. For example, after the 10-day water conditioning, the normalized  $\tau_0$  and  $G_{w-1.0}$  of the pristine fiber were 132% and 88% respectively, while those of the SiO<sub>2</sub>-coated fibers were 173% and

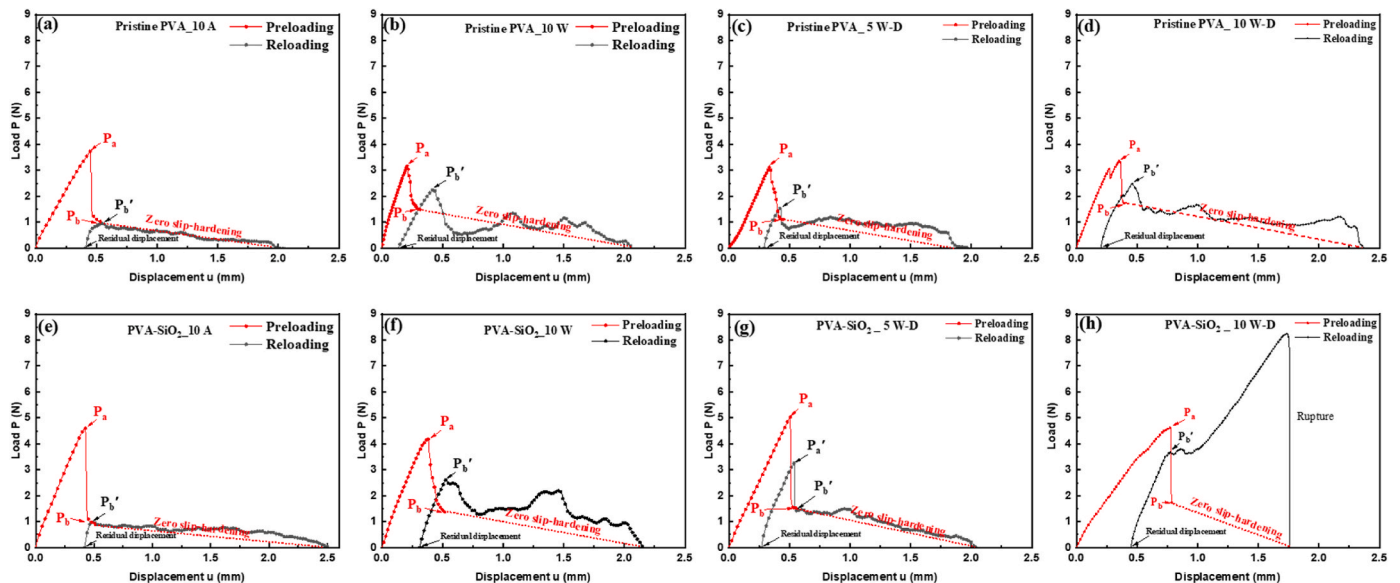


**Fig. 4.** Representative tensile load vs. fiber displacement ( $P-u$ ) curves obtained from the pre-loading, conditioning, reloading of single fiber pullout test: (a)–(d) pristine PVA fiber and (e)–(h) processed PVA fiber with SiO<sub>2</sub> nanoparticle coating.

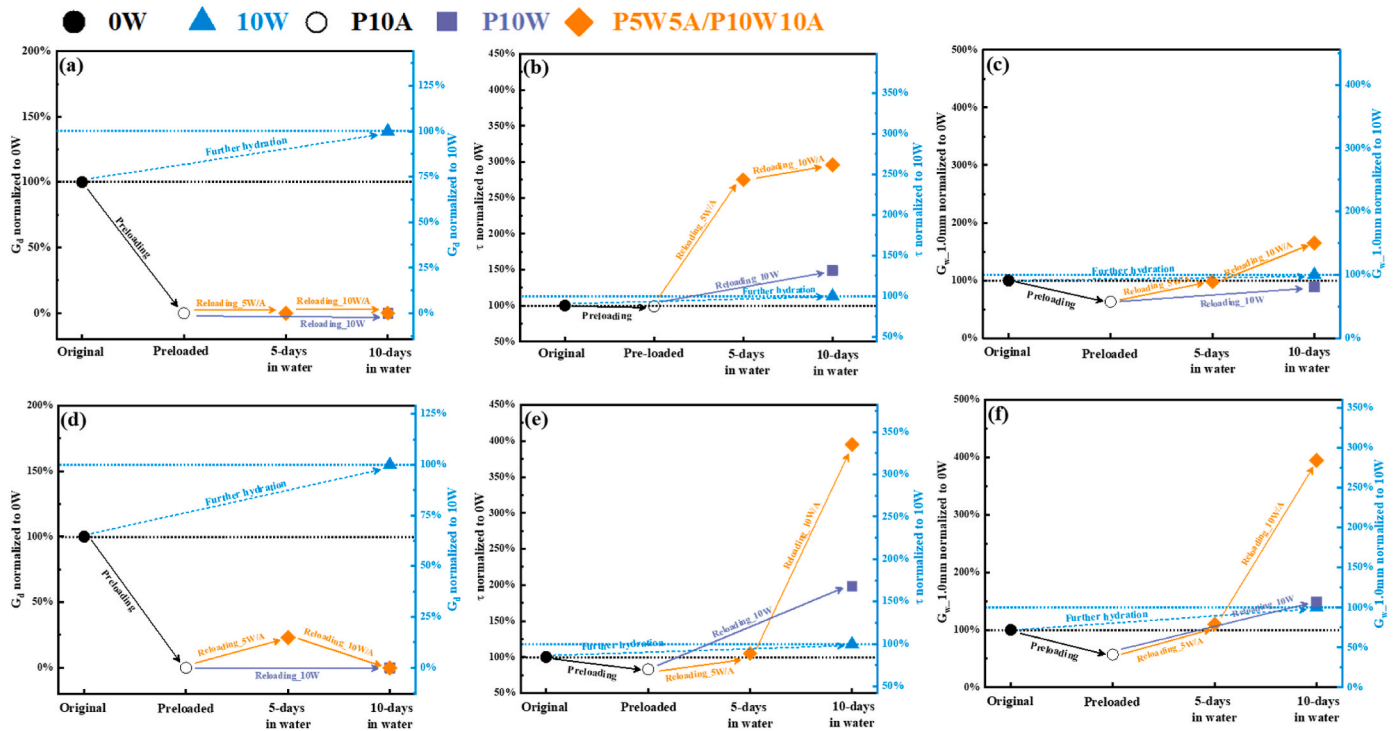


Fig. 5. Effect of the pre-loading and the subsequent healing conditions (P10W, P5W5A, and P10W) on the fiber/matrix interface properties, the normalized value to the original ones (0W) and the ones after 10 days of continued hydration (10W): (a)–(c) pristine PVA fiber and (d)–(f) processed PVA fiber with SiO<sub>2</sub> nano-particle coating.

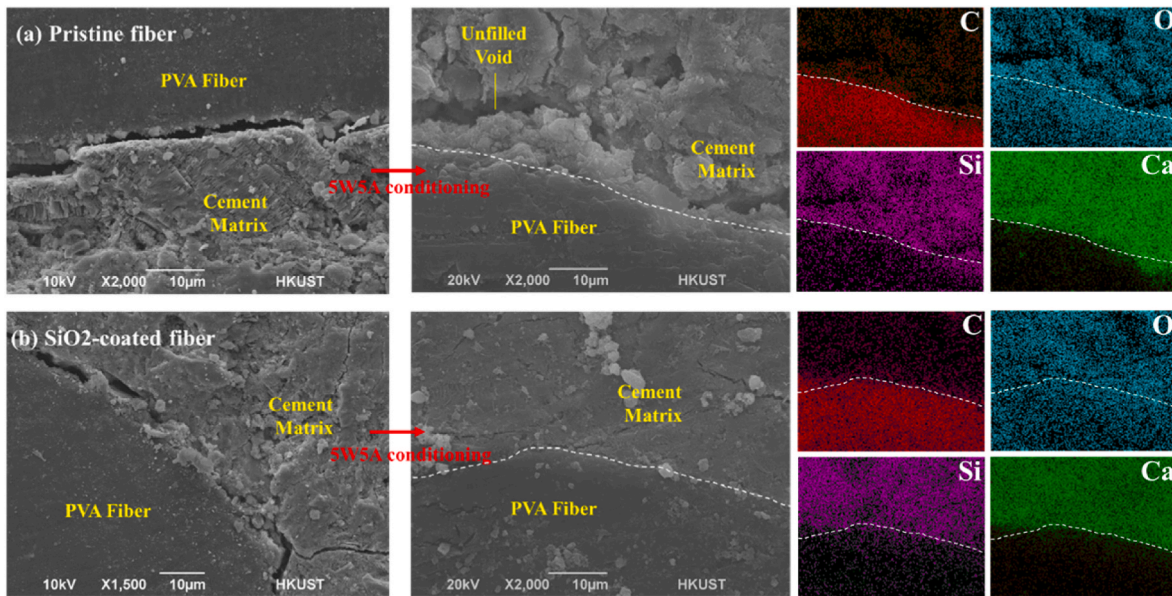


Fig. 6. The microstructure and elementary distribution of the fiber/matrix interface (cross-sectional view) after pre-loading and conditioning of 5 wetting-air cycles: (a) the pristine fiber; (b) the processed fiber.

107% respectively. For another example, after 10 wetting/air cycles, the normalized  $\tau_0$  and  $G_{w-1.0}$  of the pristine fiber were 264% and 149% respectively, while those of the SiO<sub>2</sub>-coated fibers were 345% and 284% respectively. Regarding the effect of conditioning scheme, for both pristine and processed fiber, if the total days is the same (10 days), water-only conditioning (P10W) induced slightly larger enhancement than the alternative wetting/air conditioning (P5W5A); if the days submerged in water is the same (10 days), the alternative wetting/air conditioning (P10W10A) induced significantly larger enhancement than

the water-only conditioning (P10W). These results indicate that the presence of CO<sub>2</sub> or carbonate ions is the limiting factor of interfacial enhancement and re-highlights the importance of engaging matrix crack for such enhancement to happen.

Fig. 7 compares the surface morphology of the pulled out pristine and processed fiber, which had been debonded and conditioned (10W) before the reloading. The surface of pristine fiber (Fig. 7a) is partially covered by plate-like particles, whose morphology is similar to that seen on the Ca(OH)<sub>2</sub>-contioned pristine fiber (Fig. 3a). For pristine fiber,

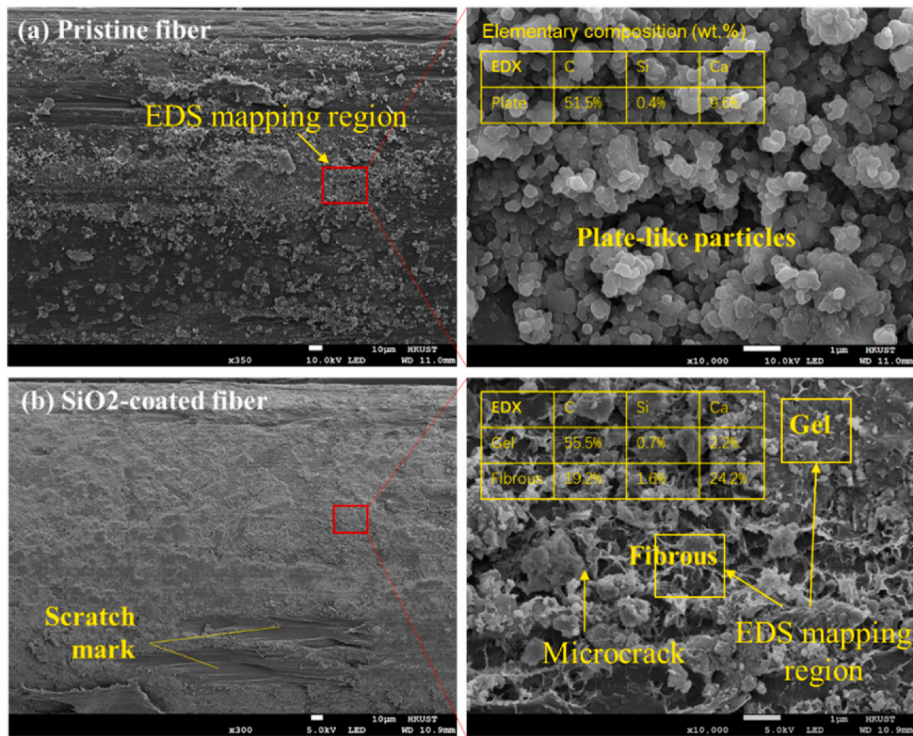


Fig. 7. The surface morphology and elementary distribution of pulled fibers after preloading and conditioning 10-day conditioning in water: (a) the pristine fiber; (b) the processed fiber.

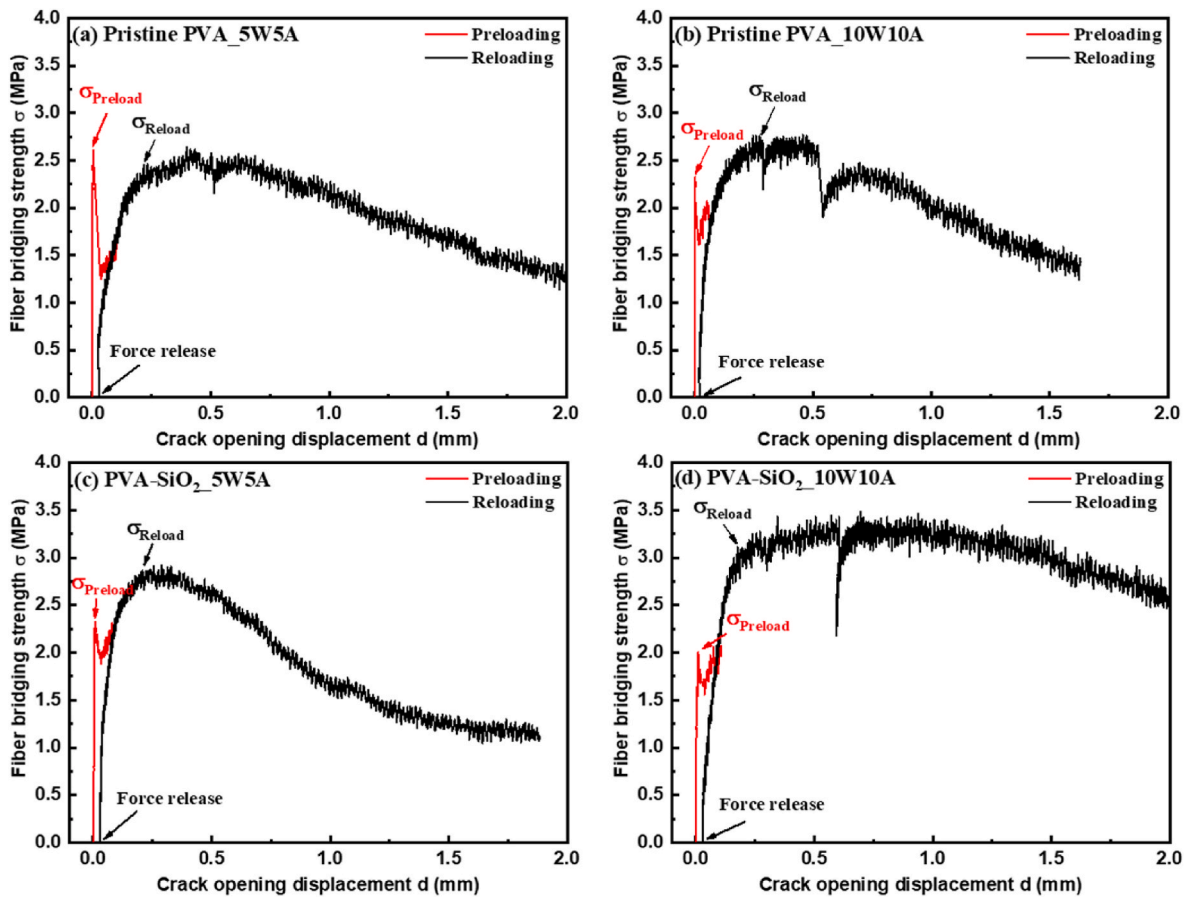


Fig. 8. Typical tensile stress vs. crack opening displacement curves from the pre-loading and the post-conditioning reloading of FRCCs made with (a, b) pristine PVA fibers and (c, d) processed PVA fibers.

there is only traceable Si, and the Ca/Si ratio is significantly higher than that of C–S–H (1.2–2.3 [46]). The observations indicate that the healing product, if there was any, did not involve new compound other than Ca(OH)<sub>2</sub> or CaCO<sub>3</sub>. The surface of processed fiber (Fig. 7b) is almost fully covered by a new layer, which is a mixture of the continuous gel-like phases and fibrous phases; the gel-like phase has a morphology that is similar to the gel-like phase seen on the Ca(OH)<sub>2</sub>-conditioned processed fiber (Fig. 3a). The gel-like phase had a Ca/Si ratio of 3.14, which is not far from that of the C–S–H; it suggests that there was new species of healing product, which is likely C–S–H induced by the SiO<sub>2</sub>. The fibrous phase had a Ca/Si ratio of 15.13, which implies that it could be a mixture of C–S–H and Ca(OH)<sub>2</sub>. Fig. 7b also suggests that the new healing product is responsible for the enhanced frictional bond, as the scratch marks are only seen on the SiO<sub>2</sub>-coated fibers. Actually, the fibrous phase may be caused by the plate-like particles “micro-scratching” the gel-like phase.

### 3.3. Preloading-and-healing-induced FRCC tensile strength enhancement

Fig. 8 shows the representative tensile stress vs. crack opening displacement ( $\sigma$ - $d$ ) curves from pre-loading and reloading of the notched FRCCs specimens. It is seen that if the fibers are coated or 10 wetting/air cycles were applied, FRCC tensile strength can be enhanced to higher than the maximum tensile stress during pre-loading, i.e., the stress right before matrix cracking. For the group SiO<sub>2</sub>-P10W10A, the tensile strength capacity is significantly enhanced from the preloading.

The FRCCs tensile properties of all the tested groups are summarized in Table 4. For the monotonically loaded groups, the equivalent elastic modulus  $E$  is calculated with Eq. (4):

$$E = \frac{\sigma_{fc}}{\varepsilon_{ca}} \quad (4)$$

where  $\sigma_{fc}$  is the tensile strength of first crack,  $\varepsilon_{ca}$  is the tensile strain at the first crack, which is the ratio of crack opening displacement at the first crack to the gauge length of LVDTs (23 mm). The  $E$  and  $\sigma_{fc}$  of the reloaded groups are normalized by that of the monotonically loaded group; the normalized value can be used to assess the healing-induced stiffness recovery and strength enhancement of FRCC. It is seen that the fiber/matrix interface healing cannot restore the tensile stiffness of the material, as it mostly relies on the matrix. However, the interface healing can significantly enhance the tensile strength, as all the tested groups have a normalized  $\sigma_{fc}$  larger than 1. The FRCCs tensile strength increases with nano-SiO<sub>2</sub> coating and conditioning cycles; the cracked-and-conditioned SiO<sub>2</sub>-P10W10A group even had a tensile strength 44.9% higher than the identically-conditioned-but-uncracked SiO<sub>2</sub>-10W10A group. These results verify the hypothesis at the beginning of this paper, that is in the presence of water, a cracked FRCC can be stronger than its uncracked counterpart.

Fig. 9 shows the microstructure of the matrix crack and the fiber/matrix interface of a fractured specimen (SiO<sub>2</sub>-P10W10A), which supports that the enhanced FRCC tensile strength is attributed to the healing-enhanced fiber/matrix interface. In Fig. 9a, the matrix crack was narrowed by wetting/air conditioning but never completely closed, which indicates the reloading properties were exclusively determined by

the fiber-bridging. In Fig. 9b, on the fracture surface a large portion of fibers were pulled out, which indicates that they must have not been ruptured by pre-loading. Healing products were found on these fiber/matrix interfaces; they should be able to contribute to the FRCC tensile strength during reloading as the fibers had not been ruptured.

### 3.4. Modeling results

Fig. 10 shows the tensile stress vs normalized COD curves of FRCCs, calculated modeling results together with the experimental results. The normalized COD was calculated as the  $d/d_0$ , where  $d_0$  is the COD corresponding to the peak of the hump. Normalized COD instead of the actual COD was used because the actual COD was overestimated in the experiment. It is clearly seen the modeling results largely capture the tensile behavior of FRCC. More importantly, the tensile strength of reloading curve is noticeably larger than that of the monotonic loading curve for both the pristine fiber- and processed fiber-reinforced groups. From the modeling the healing-induced fiber/matrix frictional bond improvement was the only contributor to the reloading strength, which verifies our hypothesis that matrix cracking can be an opportunity to make the tensile strength of FRCC higher.

## 4. Conclusions

This work experimentally and computationally explored the feasibility of achieving a higher tensile strength of FRCCs by pre-cracking and then autogenous healing. Single-fiber pullout specimens and FRCCs specimens were made with PVA fibers with or without nano-SiO<sub>2</sub> surface coating. The specimens were pre-loaded to induce fiber/matrix interface crack and/or matrix crack and then conditioned under different environmental regimes for crack healing; while the control specimens were not pre-loaded but conditioned under the same regime. Single-fiber pullout and FRCC uniaxial tensile tests were conducted to determine the effect of pre-cracking and self-healing. Micromechanics-based fiber-bridging model was also applied to demonstrate the effect of matrix precracking and fiber/matrix interface healing on the tensile behavior of FRCCs. The following conclusions can be drawn based on the experimental and modeling results.

- The nano-SiO<sub>2</sub> particles can be successfully deposited onto the PVA fiber surface via sol-gel method; the processed PVA fiber has a higher chemical reactivity with both the saturated Ca(OH)<sub>2</sub> solution, which mimics the pore solution of hardened cement matrix, and the real cement matrix. The nano-SiO<sub>2</sub> coating induced new type of healing products in larger amount at the debonded fiber/matrix interface, which has a microstructural morphology and composition that is similar to C–S–H.
- The nano-SiO<sub>2</sub> coating can enhance the original chemical bond and frictional bond between PVA fiber and cement matrix; after pre-loading and self-healing, the coating barely restores the chemical bond but induces a higher frictional bond than the original. The same healing-induced frictional bond enhancement can also be realized with a pristine PVA surface, while its magnitude is significantly smaller.

**Table 4**  
FRCCs tensile properties obtained from monotonic and preloading-reloading tests.

Fiber type	Group	Equivalent elastic modulus $E$ (GPa)	Tensile strength $\sigma_{fc}$ (MPa)	Normalized $E^a$	Normalized $\sigma_t^a$
Pristine PVA	10W10A (monotonic)	9.65 ± 2.14	2.32 ± 0.12		
	P5W5A (reloading)	0.54 ± 0.29	2.33 ± 0.30	5.6%	100.4%
	P10W10A (reloading)	0.60 ± 0.29	2.76 ± 0.13	6.2%	119.0%
Processed PVA	10W10A (monotonic)	9.83 ± 2.66	2.05 ± 0.15		
	P5W5A (reloading)	0.80 ± 0.69	2.74 ± 0.19	8.2%	133.7%
	P10W10A (reloading)	0.69 ± 0.23	2.97 ± 0.42	7.0%	144.9%

<sup>a</sup> Normalized value = the reloading of P5W5A or P10W10A to the monotonic loading of 10W10A.

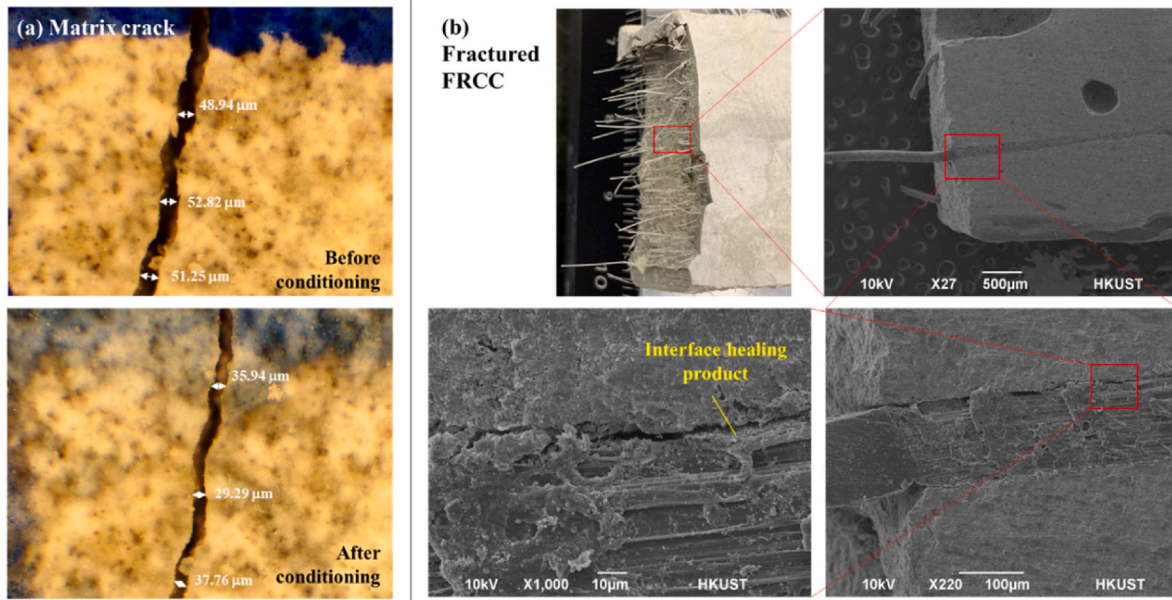


Fig. 9. Microstructure of FRCCs (P10W10A): (a) pre-loading-induced matrix crack before and after wetting-air conditioning; (b) the morphology of fractured FRCCs, the optical photo shows the crack surface where fiber pullout is the dominant fiber-bridging failure mode, the SEM images show the microstructure of the fiber/matrix interface exposed by cutting and polishing.

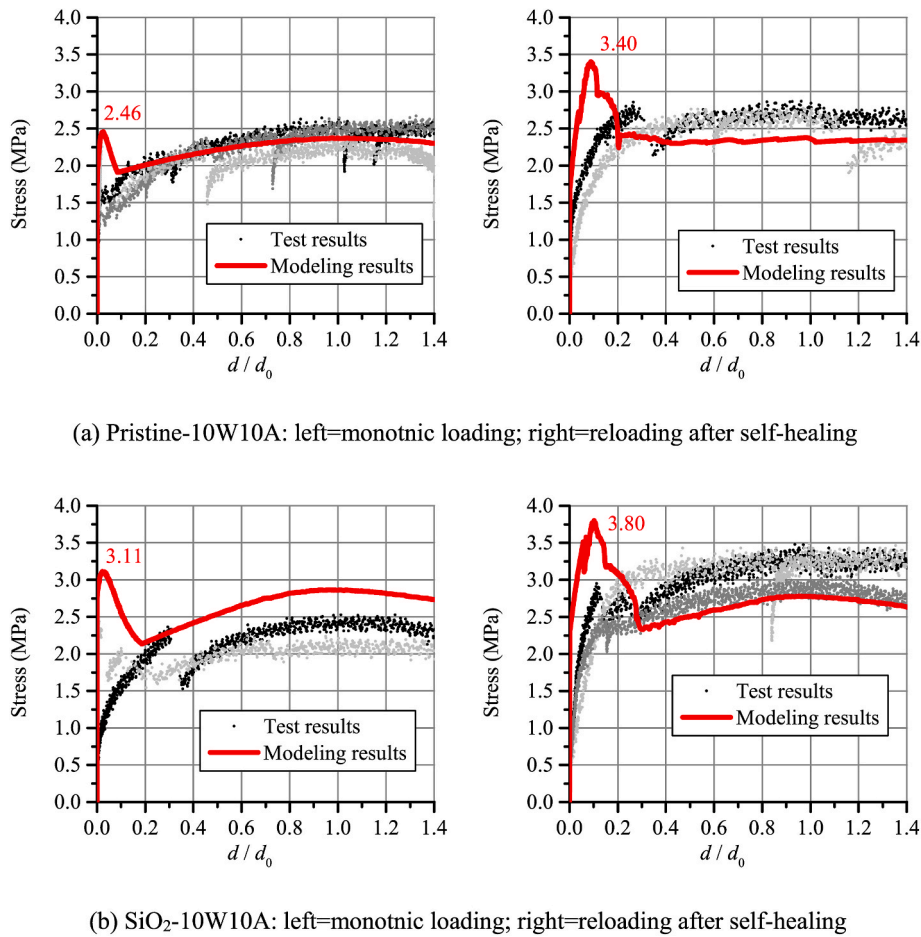


Fig. 10. The FRCCs tensile stress vs. normalized COD curves: (a) FRCC with pristine PVA fibers; (b) FRCCs with processed PVA fibers.

- For both coated and pristine fibers, the healing-induced interfacial enhancement increases with the days of water conditioning (P10W10A > P5W5A); if the days of the water conditioning is the same, alternative wetting/air conditioning can induce larger enhancement (P10W10A > P10W).
- A cracked-and-healed FRCCs can achieve a higher tensile strength than the uncracked-but-identically-conditioned control, which shows the plausibility of cracking enhance the tensile strength of concrete. Such enhancement is more efficient if the PVA fibers have a more reactive surface (e.g., the nano-SiO<sub>2</sub> coating) and they are less ruptured by the pre-loading (relatively small aspect ratio).
- Tensile behaviors of FRCCs before and after healing were simulated by micromechanics-based fiber-bridging model, and the modeling results indicate the enhancement in fiber/matrix interface bond is the dominant factor to make the tensile strength of FRCC stronger after healing.

### Declaration of competing interest

The authors declare that they have no known competing financial interests or personal relationships that could have appeared to influence the work reported in this paper.

### Data availability

Data will be made available on request.

### References

- [1] L. Petersen, L. Lohaus, M.A. Polak, Influence of freezing-and-thawing damage on behavior of reinforced concrete elements, *ACI Mater. J.* 104 (2007) 369.
- [2] C. Desmettre, J.-P. Charron, Novel water permeability device for reinforced concrete under load, *Mater. Struct.* 44 (2011) 1713–1723.
- [3] Z. Jin, X. Zhao, T. Zhao, Y. Liu, Corrosion behavior of steel bar and corrosive cracking of concrete induced by magnesium-sulfate-chloride ions, *J. Adv. Concr. Technol.* 14 (2016) 172–182.
- [4] X. Wang, Z. Yang, C. Fang, N. Han, G. Zhu, J. Tang, F. Xing, Evaluation of the mechanical performance recovery of self-healing cementitious materials-its methods and future development: a review, *Construct. Build. Mater.* 212 (2019) 400–421.
- [5] J. Ren, J. Zhang, X. Wang, D. Li, N. Han, F. Xing, Electrochemical Impedance Spectroscopy: a potential approach for detecting the breakage rate of microcapsules for self-healing cementitious materials, *Cement Concr. Compos.* 114 (2020), 103776.
- [6] Y. Zhu, Z. Zhang, X. Chen, D. Zou, X. Guan, B. Dong, Non-destructive methods to evaluate the self-healing behavior of engineered cementitious composites (ECC), *Construct. Build. Mater.* 230 (2020), 116753.
- [7] D. Snoeck, J. Dewanckele, V. Cnudde, N. De Belie, X-ray computed microtomography to study autogenous healing of cementitious materials promoted by superabsorbent polymers, *Cement Concr. Compos.* 65 (2016) 83–93.
- [8] F. Gilabert, K. Van Tittelboom, J. Van Stappen, V. Cnudde, N. De Belie, W. Van Paepegem, Integral procedure to assess crack filling and mechanical contribution of polymer-based healing agent in encapsulation-based self-healing concrete, *Cement Concr. Compos.* 77 (2017) 68–80.
- [9] K. Vijay, M. Murmu, S.V. Deo, Bacteria based self healing concrete-A review, *Construct. Build. Mater.* 152 (2017) 1008–1014.
- [10] S. Ruan, J. Qiu, Y. Weng, Y. Yang, E.-H. Yang, J. Chu, C. Unluer, The use of microbial induced carbonate precipitation in healing cracks within reactive magnesia cement-based blends, *Cement Concr. Res.* 115 (2019) 176–188.
- [11] W. Li, B. Dong, Z. Yang, J. Xu, Q. Chen, H. Li, F. Xing, Z. Jiang, Recent advances in intrinsic self-healing cementitious materials, *Adv. Mater.* 30 (2018), 1705679.
- [12] K. Van Breugel, Is there a market for self-healing cement-based materials, *Proceedings of the first international conference on self-healing materials* (2007) 1–9.
- [13] H. Huang, G. Ye, D. Damidot, Characterization and quantification of self-healing behaviors of microcracks due to further hydration in cement paste, *Cement Concr. Res.* 52 (2013) 71–81.
- [14] L.-L. Kan, H.-S. Shi, A.R. Sakulich, V.C. Li, Self-healing characterization of engineered cementitious composite materials, *ACI Mater. J.* 107 (2010) 617–624.
- [15] Y. Yang, M.D. Lepech, E.-H. Yang, V.C. Li, Autogenous healing of engineered cementitious composites under wet-dry cycles, *Cement Concr. Res.* 39 (2009) 382–390.
- [16] S. Qian, J. Zhou, M. De Rooij, E. Schlangen, G. Ye, K. Van Breugel, Self-healing behavior of strain hardening cementitious composites incorporating local waste materials, *Cement Concr. Compos.* 31 (9) (2009) 613–621.
- [17] M. Rabehi, B. Mezghiche, S. Guettala, Correlation between initial absorption of the cover concrete, the compressive strength and carbonation depth, *Construct. Build. Mater.* 45 (2013) 123–129.
- [18] V.G. Papadakis, C.G. Vayenas, M.N. Fardis, Fundamental modeling and experimental investigation of concrete carbonation, *Materials Journal* 88 (4) (1991) 363–373.
- [19] S. Ruan, J. Qiu, E.-H. Yang, C. Unluer, Influence of crack width on the stiffness recovery and self-healing of reactive magnesia-based binders under CO<sub>2</sub>-H<sub>2</sub>O conditioning, *Construct. Build. Mater.* 269 (2021), 121360.
- [20] L. Ferrara, V. Krelani, M. Carsana, A “fracture testing” based approach to assess crack healing of concrete with and without crystalline admixtures, *Construct. Build. Mater.* 68 (2014) 535–551.
- [21] S. Jacobsen, E.J. Sellevold, Self healing of high strength concrete after deterioration by freeze/thaw, *Cement Concr. Res.* 26 (1996) 55–62.
- [22] B. Hilloulin, D. Hilloulin, F. Grondin, A. Loukili, N. De Belie, Mechanical regains due to self-healing in cementitious materials: experimental measurements and micro-mechanical model, *Cement Concr. Res.* 80 (2016) 21–32.
- [23] D. Palin, H. Jonkers, V. Wiktor, Autogenous healing of sea-water exposed mortar: quantification through a simple and rapid permeability test, *Cement Concr. Res.* 84 (2016) 1–7.
- [24] Z. Zhang, Q. Zhang, V.C. Li, Multiple-scale investigations on self-healing induced mechanical property recovery of ECC, *Cement Concr. Compos.* 103 (2019) 293–302.
- [25] S. Fan, M. Li, X-ray computed microtomography of three-dimensional microcracks and self-healing in engineered cementitious composites, *Smart Mater. Struct.* 24 (2014), 015021.
- [26] V.C. Li, *Engineered Cementitious Composites (ECC): Bendable Concrete for Sustainable and Resilient Infrastructure*, Springer, 2019.
- [27] J. Yu, H.-L. Wu, C.K. Leung, Feasibility of using ultrahigh-volume limestone-calcined clay blend to develop sustainable medium-strength Engineered Cementitious Composites (ECC), *J. Clean. Prod.* 262 (2020), 121343.
- [28] H. Ma, C. Yi, C. Wu, Review and outlook on durability of engineered cementitious composite (ECC), *Construct. Build. Mater.* 287 (2021), 122719.
- [29] J. Qiu, S. He, E.-H. Yang, Autogenous healing and its enhancement of interface between micro polymeric fiber and hydraulic cement matrix, *Cement Concr. Res.* 124 (2019), 105830.
- [30] M. Lu, H. Xiao, M. Liu, X. Li, H. Li, L. Sun, Improved interfacial strength of SiO<sub>2</sub> coated carbon fiber in cement matrix, *Cement Concr. Compos.* 91 (2018) 21–28.
- [31] W. Zhang, X. Zou, F. Wei, H. Wang, G. Zhang, Y. Huang, Y. Zhang, Grafting SiO<sub>2</sub> nanoparticles on polyvinyl alcohol fibers to enhance the interfacial bonding strength with cement, *Compos. B Eng.* 162 (2019) 500–507.
- [32] Y. Liu, B. Wu, J. Qiu, A depth-dependent fiber-bridging model to predict the tensile properties recovery induced by the self-healing of strain-hardening cementitious composites, *Proceeding of SHCCS 24* (2022).
- [33] Z. Lu, J. Yao, C.K. Leung, Using graphene oxide to strengthen the bond between PE fiber and matrix to improve the strain hardening behavior of SHCC, *Cement Concr. Res.* 126 (2019), 105899.
- [34] X. Yang, L. Zhu, Y. Chen, B. Bao, J. Xu, W. Zhou, Controlled hydrophilic/hydrophobic property of silica films by manipulating the hydrolysis and condensation of tetraethoxysilane, *Appl. Surf. Sci.* 376 (2016) 1–9.
- [35] J. Zuo, B. Wu, C. Luo, B. Dong, F. Xing, Preparation of MgAl layered double hydroxides intercalated with nitrite ions and corrosion protection of steel bars in simulated carbonated concrete pore solution, *Corrosion Sci.* 152 (2019) 120–129.
- [36] B. Wu, J. Qiu, Enhancing the hydrophobic PP fiber/cement matrix interface by coating nano-AIOOH to the fiber surface in a facile method, *Cement Concr. Compos.* 125 (2022), 104297.
- [37] C. Redon, V.C. Li, C. Wu, H. Hoshino, T. Saito, A. Ogawa, Measuring and modifying interface properties of PVA fibers in ECC matrix, *J. Mater. Civ. Eng.* 13 (6) (2001) 399–406.
- [38] H. Fujiwara, M. Shibayama, J.H. Chen, S. Nomura, Preparation of high-strength poly (vinyl alcohol) fibers by crosslinking wet spinning, *J. Appl. Polym. Sci.* 37 (5) (1989) 1403–1414.
- [39] L. Black, K. Garbev, P. Stemmermann, K.R. Hallam, G.C. Allen, Characterisation of crystalline C-S-H phases by X-ray photoelectron spectroscopy, *Cement Concr. Res.* 33 (6) (2003) 899–911.
- [40] L. Black, K. Garbev, I. Gee, Surface carbonation of synthetic C-S-H samples: a comparison between fresh and aged C-S-H using X-ray photoelectron spectroscopy, *Cement Concr. Res.* 38 (2008) 745–750.
- [41] E.-H. Yang, S. Wang, Y. Yang, V.C. Li, Fiber-bridging constitutive law of engineered cementitious composites, *J. Adv. Concr. Technol.* 6 (2008) 181–193.
- [42] Z. Lin, T. Kanda, V.C. Li, On interface property characterization and performance of fiber reinforced cementitious composites, *Concrete Science and Engineering* 1 (1999) 173–184.
- [43] Z. Pi, H. Xiao, R. Liu, M. Liu, H. Li, Effects of brass coating and nano-SiO<sub>2</sub> coating on steel fiber–matrix interfacial properties of cement-based composite, *Compos. B Eng.* 189 (2020), 107904.
- [44] Z. Pi, H. Xiao, J. Du, M. Liu, H. Li, Interfacial microstructure and bond strength of nano-SiO<sub>2</sub>-coated steel fibers in cement matrix, *Cement Concr. Compos.* 103 (2019) 1–10.
- [45] X. Liu, P. Feng, X. Shu, Q. Ran, Effects of highly dispersed nano-SiO<sub>2</sub> on the microstructure development of cement pastes, *Mater. Struct.* 53 (1) (2020) 1–12.
- [46] I.G. Richardson, The nature of C-S-H in hardened cements, *Cement Concr. Res.* 29 (1999) 1131–1147.